



## Dual polarity accurate mass calibration for electrospray ionization and matrix-assisted laser desorption/ionization mass spectrometry using maltooligosaccharides

Brian H. Clowers<sup>a</sup>, Eric D. Dodds<sup>a</sup>, Richard R. Seipert<sup>a</sup>, Carlito B. Lebrilla<sup>a,b,\*</sup>

<sup>a</sup> Department of Chemistry, University of California, Davis, Davis, CA 95616, USA

<sup>b</sup> School of Medicine, University of California, Davis, Davis, CA 95616, USA

### ARTICLE INFO

#### Article history:

Received 22 March 2008

Available online 16 July 2008

#### Keywords:

Mass calibration

Electrospray ionization

Matrix-assisted laser desorption/ionization

Oligosaccharide

Porous-graphitized carbon

Infrared multiphoton dissociation

### ABSTRACT

In view of the fact that memory effects associated with instrument calibration hinder the use of many mass-to-charge ( $m/z$ ) ratios and tuning standards, identification of robust, comprehensive, inexpensive, and memory-free calibration standards is of particular interest to the mass spectrometry community. Glucose and its isomers are known to have a residue mass of 162.05282 Da; therefore, both linear and branched forms of polyhexose oligosaccharides possess well-defined masses, making them ideal candidates for mass calibration. Using a wide range of maltooligosaccharides (MOSs) derived from commercially available beers, ions with  $m/z$  ratios from approximately 500 to 2500 Da or more have been observed using Fourier transform ion cyclotron resonance mass spectrometry (FT-ICR-MS) and time-of-flight mass spectrometry (TOF-MS). The MOS mixtures were further characterized using infrared multiphoton dissociation (IRMPD) and nano-liquid chromatography/mass spectrometry (nano-LC/MS). In addition to providing well-defined series of positive and negative calibrant ions using either electrospray ionization (ESI) or matrix-assisted laser desorption/ionization (MALDI), the MOSs are not encumbered by memory effects and, thus, are well-suited mass calibration and instrument tuning standards for carbohydrate analysis.

© 2008 Elsevier Inc. All rights reserved.

Accurate and precise mass-to-charge ( $m/z$ )<sup>1</sup> calibration is the fundamental tenet from which all subsequent mass spectrometry (MS) measurements and results are derived. Therefore, it is of great importance that compounds used for calibration are well characterized and produce clearly defined  $m/z$  ratios in the range of analytical interest. When possible, internal calibration is preferred over external methods; however, in practice, external calibration is often the only available method. A suitable calibrant behaves chemically in a manner that closely relates to the analyte throughout all stages of an experiment. An isotopically labeled version of the analyte is ideal, although such compounds are not always available

and may be prohibitively expensive. To accommodate the needs of the many ionization sources compatible with MS, a wide range of calibration methods and standards have been developed.

Perfluorinated organics, such as perfluorokerosene (PFK) and perfluorotributylamine (FC-43), have been used extensively with electron impact (EI) and chemical ionization (CI) and are well suited to the  $m/z$  range associated with typical gas chromatographic analysis ( $<m/z$  1000) [1,2]. However, these compounds are often plagued by memory effects that interfere with subsequent analyses. Calibration compounds for fast atom bombardment (FAB) have also included perfluorinated species, specifically perfluoroalkylphosphazine (Ultramark 1621) [3], polypropylene glycol (PPG) [4], polyethylene glycol (PEG) [5], poly(ethylene/propylene) oxides [6], and iodide salts [7]. These compounds have an extended mass range (up to  $m/z \sim 2000$ ) but are also encumbered by source contamination following calibration. Although iodide salt solutions may be tailored to reduce memory effects, these salts must be clustered with polymeric organics to obtain high  $m/z$  ratios (i.e.,  $m/z > 10,000$ ) [8]. Unfortunately, these polymeric organics once again introduce the problems associated with calibrant memory effects.

The need for broad mass range, dual polarity, carryover-free calibrants has rapidly expanded with the concurrent rise of

\* Corresponding author. Address: Department of Chemistry, University of California, Davis, Davis, CA 95616, USA. Fax: +1 530 754 5609.

E-mail address: [cblebrilla@ucdavis.edu](mailto:cblebrilla@ucdavis.edu) (C.B. Lebrilla).

<sup>1</sup> Abbreviations used:  $m/z$ , mass-to-charge; MS, mass spectrometry; PFK, perfluorokerosene; FC-43, perfluorotributylamine; EI, electron impact; CI, chemical ionization; FAB, fast atom bombardment; Ultramark 1621, perfluoroalkylphosphazine; PPG, polypropylene glycol; PEG, polyethylene glycol; ESI, electrospray ionization; MALDI, matrix-assisted laser desorption/ionization; MOS, maltooligosaccharide; DP, degrees of polymerization; SPE, solid-phase extraction; PGC, porous graphitized carbon; nano-LC, nano-liquid chromatography; FT-ICR-MS, Fourier transform ion cyclotron resonance mass spectrometry; SWIFT, stored waveform inverse Fourier transform; IRMPD, infrared multiphoton dissociation; TOF-MS, time-of-flight mass spectrometry; DHB, 2,5-dihydroxybenzoic acid.

electrospray ionization (ESI) [9], matrix-assisted laser desorption/ionization (MALDI) [10], and efforts focusing on systems biology using MS. Many of the calibration compounds used for FAB have been ported to these newer ionization sources, although their drawbacks have been only slightly mitigated [8–13]. To mimic actual samples and minimize memory effects, mixtures of highly purified peptides and proteins have proven to be extremely effective for higher mass calibration, especially trypsin autolysis peptides [14]. Although these standards are adequate for proteomics efforts, the instrumental parameters necessary for their observation are often varied and highly specific. For example, instrumental operating conditions used for calibration using water clusters can be drastically different from those necessary for analysis (e.g., low temperature source conditions are often necessary to observe water clustering) [15]. Being no less important than proteomics, the areas of glycomics and glyco-proteomics also require appropriate standards for mass calibration and instrument tuning. In contrast to peptides and proteins, carbohydrates are usually observed as singly charged species using ESI and MALDI in both positive and negative modes, and they often require different operating conditions. Despite being one of the most ubiquitous classes of organic compounds on the earth, naturally occurring and synthetic glycan standards are often difficult to prepare and are exceedingly expensive, thereby reducing their utility as everyday mass and tuning calibrants. Our efforts to identify suitable carbohydrate standards for mass calibration and instrumental tuning have identified a commonly available source of highly specific carbohydrates in beer.

Prior to fermentation the primary sources of carbohydrates in wort include starch, pentosan,  $\beta$ -glucan, and cell wall fragments; however, once fermentation begins, these carbohydrates are enzymatically digested to form maltooligosaccharides (MOSs) in beer with degrees of polymerization (DP) ranging from 3 to 40 units [16,17]. Carbohydrates with DPs of 3 or less are most often metabolized to form the primary products of fermentation, ethyl alcohol, and carbon dioxide, with the remaining carbohydrates residing in solution [17,18]. Using a wide variety of analytical approaches, such as capillary electrophoresis [19], liquid chromatography [16,20], fluorescence-assisted carbohydrate electrophoresis [21], high-performance anion exchange chromatography, nuclear magnetic resonance spectroscopy [16,22], and MS, it has been long established that the soluble fraction of beer carbohydrates is composed of a broad array of hexose polysaccharides. Because glucose and its isomers possess the same residue mass (theoretical monoisotopic mass: 162.05282 Da), by extension polymeric molecules built from these monomers have well-defined masses and are prime selections for mass calibration.

Using a number of commercially available beers as MOS sources, this article outlines the general instrumental operating parameters necessary to use the MOSs derived from beer as mass calibrants and tuning standards for carbohydrate mass spectrometry. The MOSs found in beer may be observed in both ion polarities using either ESI or MALDI, and they span a broad mass range ( $m/z \geq 500$ –2500) that could not otherwise be achieved due to the commercial unavailability of pure, higher order MOSs. Moreover, beer MOSs are easily obtained, relatively inexpensive, and consistently distributed across the mass scale, and they do not suffer from memory effects common with many polymeric or clustering mass calibrants.

## Materials and methods

### Chemicals and materials

A total of 12 commercially available beers served as the MOS sources used in this study. Prior to dilution, each beer sample

was degassed (by either bath sonication or sparging with nitrogen gas until no noticeable carbonation remained) and centrifuged (maximum speed in a standard analytical centrifuge for several minutes), and the supernatant was decanted to remove any particulates remaining from the brewing process. For infusion experiments and flow injection analysis using nano-ESI ( $\sim 200$  nL/min), each ale or lager beer was diluted 2500 times (unless otherwise specified) in a 50:50 water/acetonitrile solution containing 0.1% formic acid. For MALDI analysis, each sample was diluted 100 times in a 50:50 water/acetonitrile solution. An enriched MOS preparation was also isolated from beer using solid-phase extraction (SPE) with porous graphitized carbon (PGC, Thermo HyperSep HyperCarb) [23]. A 100- $\mu$ l aliquot of degassed beer supernatant was loaded onto the cartridge and washed with three cartridge volumes of deionized water. The oligosaccharides were eluted with 1 ml of a 50:50 acetonitrile/water solution and further diluted as described above for ESI and MALDI analysis. To enhance the abundance of the sodiated molecular ions in positive mode ESI, PGC-purified MOS mixtures were treated with 10  $\mu$ M NaCl.

### Chromatography and flow injection analysis

When performing nano-liquid chromatography (nano-LC), each sample was diluted using the initial gradient conditions described below. Nano-LC was performed at 250 nL/min using a 10-cm custom-packed PGC stationary phase within a fused silica capillary column (75  $\mu$ m i.d.  $\times$  365  $\mu$ m o.d., Polymicro Technology, Phoenix, AZ, USA) [24]. The linear gradient using degassed 18 M $\Omega$  water (solvent A) and acetonitrile (solvent B), both with 0.1% formic acid, was delivered using an Eksigent one-dimensional nano-LC pump (Livermore, CA, USA). The gradient profile was as follows: 0 min, 98% A; 10 min, 98% A; 50 min, 60% A; 70 min, 20% A; 80 min, 20% A. Flow injection analysis was performed with 50% A at a flow rate of 500 nL/min.

### Electrospray ionization mass spectrometry

For analysis by Fourier transform ion cyclotron resonance mass spectrometry (FT-ICR-MS), a PicoView nano-ESI stage (New Objective, Woburn, MA, USA) was held at  $\pm 1800$  to 2400 V and used to electrospray the beer solutions into a 9.4 Tesla instrument equipped with external ion accumulation and mass filtration (IonSpec QFT, Irvine, CA, USA). Prior to entering the vacuum stage of the mass spectrometer, the electrosprayed ions passed through a sample cone with a 390- $\mu$ m aperture and traversed a Z-spray (off-axis) ion source (Waters, Manchester, UK). In addition to the sample cone potential ( $\pm 60$ –115 V), the other key component of this ion source was the cone extractor held at  $\pm 15$  V. Once through the atmospheric pressure interface, ions were externally accumulated in the hexapole (operated at 980 kHz, 200 V base-to-peak amplitude) for up to 4 s prior to injection to the ICR cell via a quadrupole ion guide (operated at 980 kHz, 275 V base-to-peak amplitude). After identifying candidate  $m/z$  values for tandem MS, the FT-ICR control software was used to trigger stored waveform inverse Fourier transform (SWIFT) isolation prior to pulsing a 10.6- $\mu$ m CO<sub>2</sub> laser (Parallax Laser, Waltham, MA, USA) used for infrared multiphoton dissociation (IRMPD). To accommodate the disperse ion cloud, the laser beam was expanded to 0.5 cm using an adjustable beam expander (Synrad Laser, Mukilteo, WA, USA) and was directed toward the center of the ICR cell through a BaF<sub>2</sub> window (Bicron, Newbury, OH, USA). Product ion formation was optimized by varying the IRMPD laser pulse from 500 to 2000 ms. All of the mass spectra shown correspond to the fast Fourier transformation of a 1.024-s transient signal acquired using an ADC rate of 1 MHz. The transform was performed after

applying a Blackman window for apodization and appending a one-order zero fill.

Analysis by time-of-flight mass spectrometry (TOF–MS) was accomplished using an Agilent Technologies 6200 series HPLC chip/TOF–MS (Santa Clara, CA, USA). MOS samples were delivered by a syringe pump at a flow rate of 300 nl/min. The sample flow was interfaced to the nano-ESI ion source using an infusion-only chip. The ESI capillary potential was held at 1800 V, the fragmentor potential was held at 425 V, and the skimmer potential was held at 160 V. Mass analysis was performed by orthogonal acceleration reflectron TOF in positive ion mode with an acquisition rate of approximately 1 scan/s.

#### Matrix-assisted laser desorption/ionization mass spectrometry

MOS samples were co-spotted with the appropriate matrix to produce either positive or negative ions using MALDI. For the positive mode, a matrix solution containing 50  $\mu\text{g}/\mu\text{l}$  2,5-dihydroxybenzoic acid (DHB) and 5  $\mu\text{M}$  NaCl was prepared in a 50:50 acetonitrile/water solution, and 1  $\mu\text{l}$  of this mixture was co-spotted with 1  $\mu\text{l}$  of the analyte solution. For the negative mode, spots were prepared essentially according to Suzuki and coworkers [25] using harmine (7-methoxy-1-methyl-9H-pyrido[3,4-b]indole, Sigma–Aldrich, St. Louis, MO, USA) as the matrix (prepared at a concentration of 5  $\mu\text{g}/\mu\text{l}$  in a 50:50 acetonitrile/water solution)

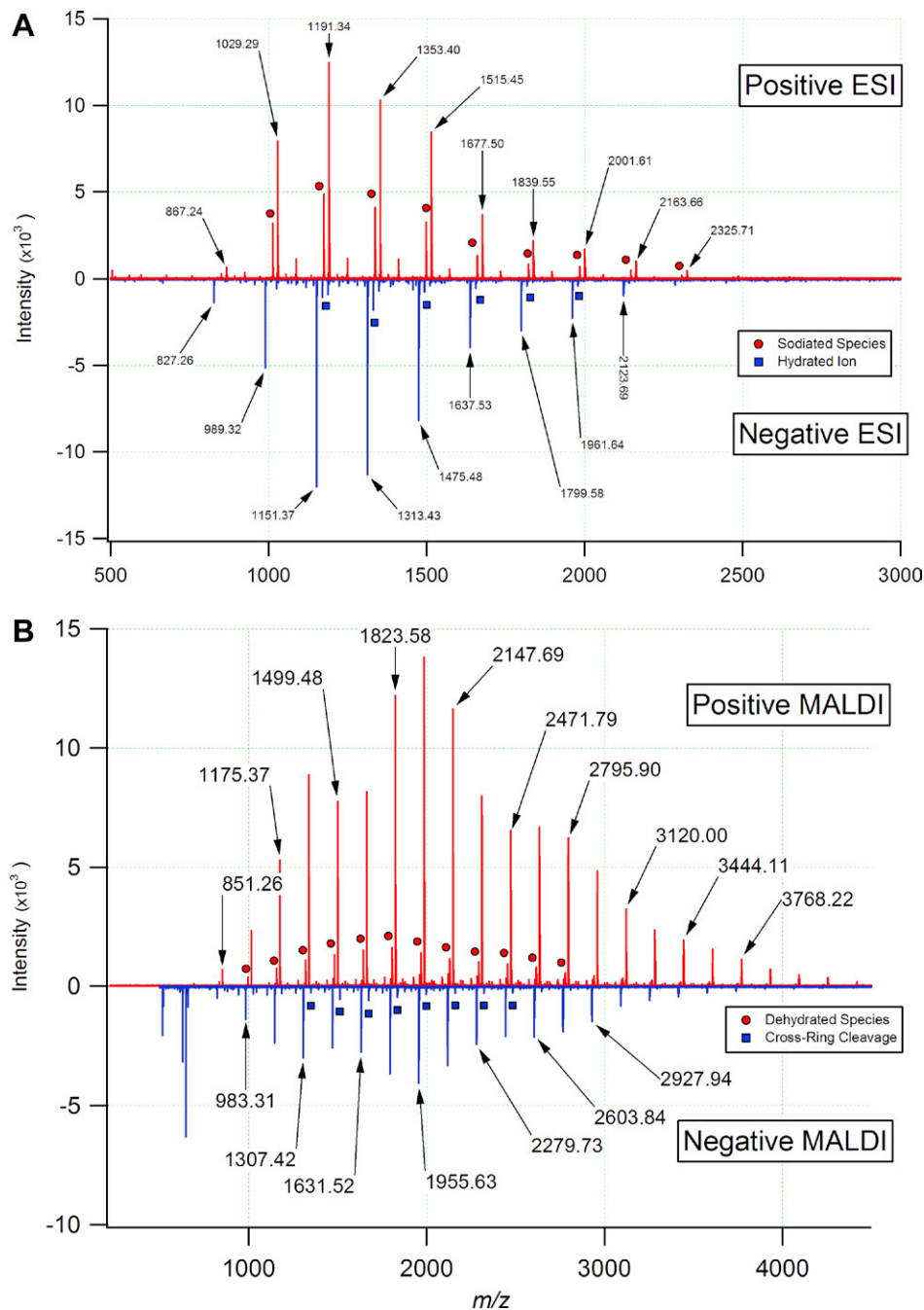


**Fig. 1.** Comparison of the commonly observed positively and negatively charged MOSs found in beer generated using ESI and MALDI with mass analysis by FT–ICR–MS. (A) Whereas the positive mode ESI was dominated by sodium (circles) and potassium adducts (most abundant series), the carbohydrates observed in the negative mode were observed primarily as deprotonated  $[M-H]^-$  species and, to a very small extent, a hydrated series (squares). (B) For MALDI analysis,  $[M+Na]^+$  ions were the most abundant series observed, whereas in the negative mode the major series corresponded to products of two sequential cross-ring cleavages (the two most abundant MOS series).

with a comatrix of  $\text{NH}_4\text{Cl}$  (prepared at a concentration of 100 mM, aqueous). Each 1- $\mu\text{l}$  sample spot was treated with 1  $\mu\text{l}$  of the harmine solution and 1  $\mu\text{l}$  of the  $\text{NH}_4\text{Cl}$  solution. All MALDI spots were prepared on a stainless-steel sample target and were vacuum-dried. MALDI-MS was performed with a 7.0 Tesla, external source FT-ICR instrument (IonSpec Pro MALDI). Ions from 5 to 25 laser pulses (Nd:YAG, 355 nm) were accumulated in a hexapole (operated at 925 kHz, 200 V base-to-peak amplitude) and collisionally cooled using a controlled leak of nitrogen into the hexapole chamber. Ions were then injected into the ICR cell via a quadrupole ion guide (operated at 925 kHz, 500 V base-to-peak amplitude). Detection parameters were essentially the same as those specified for ESI-FT-ICR analysis.

## Results and discussion

Of the 12 beers examined in this study, representative MOS spectra acquired using both nano-ESI and MALDI ionization sources in both polarities are shown in Fig. 1. These spectra demonstrate the evenly spaced ( $\Delta m/z$  162.05282) yet wide range of  $m/z$  values observed for the MOSs in beer. It should be noted that each of the nano-ESI beer spectra shown (Fig. 1A) was acquired for samples diluted 2500-fold and required only minimal flushing to eliminate the MOSs from the system. Given the availability and lack of carryover effects associated with MOSs, the observed signal-to-noise ratio could be adjusted by simply altering the MOS dilution factor or by changing the ion accumulation time. To assess the relative purity of each beer sample and remove any possible interferents, a carbohydrate enrichment step was performed using SPE with PGC as described above. Comparison of the enriched fraction with the diluted beer sample indicated that no marked benefit was afforded by the SPE enrichment procedure. Consequently, the commercial beer samples were then used without additional purification.

A well-known feature of carbohydrates is their strong affinity for alkali earth metals, particularly sodium and potassium [26]. The MOS ions observed in this study were no exception to this trend, with the two most prominent species observed by positive ion nano-ESI being sodium  $[\text{M}+\text{Na}]^+$  and potassium  $[\text{M}+\text{K}]^+$  adducts (Fig. 1A, upper trace). For the beer samples examined, small variations in the relative abundance of the two adducts were observed and were attributed to the varying mineral content of the water used during the brewing process. Lower abundance MOS series were also observed in the positive ESI mode; however, their restricted  $m/z$  range limited their use as a calibration series. The MOS ions produced by positive mode MALDI were observed almost exclusively as  $[\text{M}+\text{Na}]^+$  adducts due to the doping of the sample spots with NaCl (Fig. 1B, upper trace). A previous article examining beer MOSs reported DP up to 40 (6500.1234 Da, monoisotopic neutral mass) [16,27]. In the current work, the largest MOS observed using nano-ESI corresponded to a DP of 21 (3421.1198 Da, monoisotopic neutral mass), and the largest MOS observed by MALDI corresponded to a DP of 27 (4393.4367 Da). The enhanced  $m/z$  range observed using MALDI as compared with ESI was attributed to the absence of an atmospheric pressure interface and differences in the ion transfer optics. No doubt, MOSs with higher DP are present in beer; however, their low abundance and ion bandpass limitations hindered the observation of higher order MOSs (i.e.,  $\text{DP} > 27$ ). A list of theoretical  $m/z$  values and core accurate masses used in the calculation of MOS  $m/z$  is reported in Table 1.

Whereas the positive mode spectra of electrosprayed beer carbohydrates were dominated by sodium and potassium adducts, the MOS species in the negative mode were most commonly deprotonated  $[\text{M}-\text{H}]^-$ , as seen in the lower trace of Fig. 1A. Compared with the results obtained for the other ionization and source configurations, the signal intensity of the negatively charged MOSs using MALDI with the harmine/ $\text{NH}_4\text{Cl}$  matrix was significantly less. Com-

**Table 1**  
Theoretical monoisotopic masses of beer MOSs

Species	Formula	Mass (Da)					
Hexose residue	$\text{C}_6\text{H}_{10}\text{O}_5$	162.0528					
Water	$\text{H}_2\text{O}$	18.0106					
Sodium ion	$\text{Na}^+$	22.9892					
Potassium ion	$\text{K}^+$	38.9632					
Proton	$\text{H}^+$	1.0073					
Cross-ring loss $\text{R}_1$	$\text{C}_4\text{H}_8\text{O}_4$	120.0423					
Cross-ring loss $\text{R}_2$	$\text{CH}_2\text{O}$	30.0106					
MOS DP	$[\text{M}+\text{Na}]^+$	$[\text{M}+\text{K}]^+$	$[\text{M}-\text{H}]^-$	$[\text{M}-\text{R}_1-\text{H}]^-$	$[\text{M}-\text{R}_2-\text{H}_2\text{O}-\text{H}]^-$	$[\text{M}-\text{R}_1-\text{R}_2-\text{H}_2\text{O}-\text{H}]^-$	
3	527.1582	543.1322	503.1617	383.1195	455.1406	335.0984	
4	689.2111	705.1850	665.2146	545.1723	617.1934	497.1512	
5	851.2639	867.2378	827.2674	707.2251	779.2463	659.2040	
6	1013.3167	1029.2906	989.3202	869.2779	941.2991	821.2568	
7	1175.3695	1191.3435	1151.3730	1031.3308	1103.3519	983.3096	
8	1337.4223	1353.3963	1313.4258	1193.3836	1265.4047	1145.3625	
9	1499.4752	1515.4491	1475.4787	1355.4364	1427.4575	1307.4153	
10	1661.5280	1677.5019	1637.5315	1517.4892	1589.5104	1469.4681	
11	1823.5808	1839.5547	1799.5843	1679.5420	1751.5632	1631.5209	
12	1985.6336	2001.6076	1961.6371	1841.5949	1913.6160	1793.5737	
13	2147.6864	2163.6604	2123.6899	2003.6477	2075.6688	1955.6266	
14	2309.7393	2325.7132	2285.7428	2165.7005	2237.7216	2117.6794	
15	2471.7921	2487.7660	2447.7956	2327.7533	2399.7745	2279.7322	
16	2633.8449	2649.8188	2609.8484	2489.8061	2561.8273	2441.7850	
17	2795.8977	2811.8717	2771.9012	2651.8590	2723.8801	2603.8378	
18	2957.9505	2973.9245	2933.9540	2813.9118	2885.9329	2765.8907	
19	3120.0034	3135.9773	3096.0069	2975.9646	3047.9857	2927.9435	
20	3282.0562	3298.0301	3258.0597	3138.0174	3210.0386	3089.9963	
21	3444.1090	3460.0829	3420.1125	3300.0702	3372.0914	3252.0491	
22	3606.1618	3622.1358	3582.1653	3462.1231	3534.1442	3414.1019	
23	3768.2146	3784.1886	3744.2181	3624.1759	3696.1970	3576.1548	
24	3930.2675	3946.2414	3906.2710	3786.2287	3858.2498	3738.2076	
25	4092.3203	4108.2942	4068.3238	3948.2815	4020.3027	3900.2604	
26	4254.3731	4270.3470	4230.3766	4110.3343	4182.3555	4062.3132	
27	4416.4259	4432.3999	4392.4294	4272.3872	4344.4083	4224.3660	
28	4578.4787	4594.4527	4554.4822	4434.4400	4506.4611	4386.4189	
29	4740.5316	4756.5055	4716.5351	4596.4928	4668.5139	4548.4717	
30	4902.5844	4918.5583	4878.5879	4758.5456	4830.5668	4710.5245	

parison of the relative intensities of the major ion peaks in the positive and negative modes reflects an approximately threefold difference in sensitivity. To compensate for the lower sensitivity of negative mode MALDI for MOS analysis, ions were accumulated from 25 laser shots as opposed to 5 shots for positive mode MALDI. Although still useful for instrument tuning and calibration, the observation of intact MOS ions in the negative mode using MALDI was not attainable due to the relative instability of these compounds in negative mode. Previous studies of negatively charged nonreducing neutral oligosaccharides have indicated that the chloride  $[\text{M}+\text{Cl}]^-$  adducts formed with the use of harmine/ $\text{NH}_4\text{Cl}$  matrix readily decay to form deprotonated  $[\text{M}-\text{H}]^-$  ions [28,29]. These deprotonated ions are subject to further in-source and post-source decay mechanisms, including cross-ring cleavage. Our experiments provide further confirmation of this behavior given that the negatively charged beer MOS ions generated by MALDI corresponded to two series of cross-ring cleavage products. The first of these series was equivalent to a deprotonated molecular ion that had lost 48.0211 Da (i.e.,  $[\text{M}-\text{CH}_2\text{O}-\text{H}_2\text{O}-\text{H}]^-$ ) and was consistent with the observations of Yamagaki and coworkers [29]. This series was represented by the minor signals shown in the lower trace of Fig. 1B. The second series corresponded to a further degradation of ions from the first series with the additional loss of 120.0423 Da to produce  $[\text{M}-\text{C}_4\text{H}_8\text{O}_4-\text{CH}_2\text{O}-\text{H}_2\text{O}-\text{H}]^-$  fragments. These double-cleavage products constitute the major series of signals seen in the lower trace of Fig. 1B.

Using the nomenclature of Doman and Costello [30], the post-source decay ions can be described as products of successive fragmentations of the X and A types. Calibrating the spectrum on the

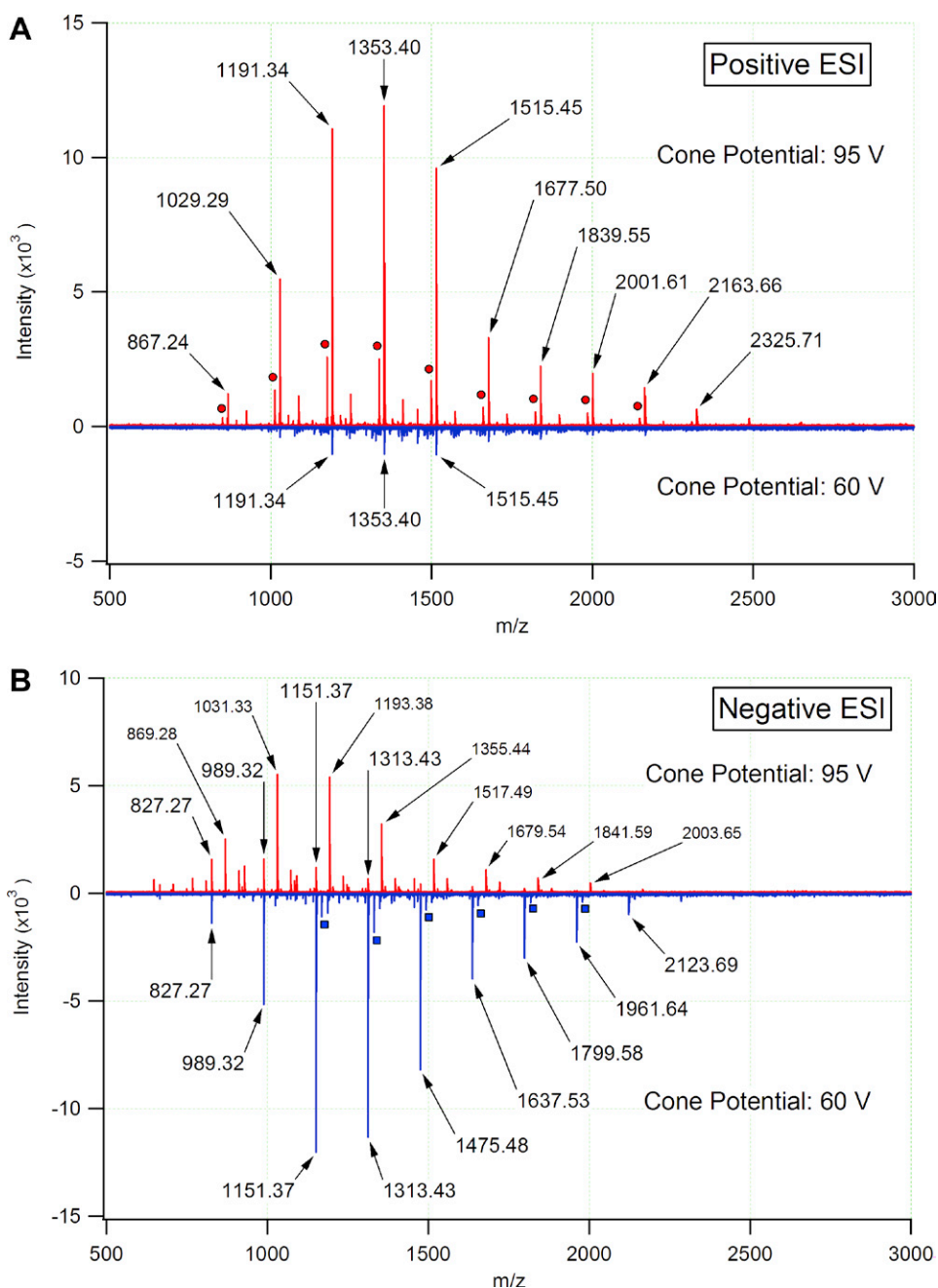


**Fig. 2.** Influence of ESI cone voltage on the relative abundance and observed MOS ions in both the positive and negative modes with mass analysis by FT-ICR-MS. (A) In the positive mode, the type of adduct observed was relatively unchanged with cone potential; however, total ion abundances were highly dependent on this value. (B) Higher cone potentials in the negative mode induced fragmentation (labeled in smaller font), whereas lower cone potentials yielded the deprotonated species. For the MOS sample shown, the positive mode was dominated by potassiated adducts, with a smaller series corresponding to the sodiated adducts (circles). Additional series were observed; however, the relative abundance of these series limits their utility as calibrants.

minor series of fragments, the masses of the major ion series were found to agree with these assignments to within  $\sim 3$  ppm root mean square mass error, thereby supporting the hypothesis that the ions are related via cross-ring fragmentation. Although the negatively charged MOS ions produced by MALDI are prone to significant fragmentation due to the inherent instability of these species, their usefulness as mass calibrants is not diminished because the elemental composition of the observed ions remains known.

The propensity of the negatively charged MOS ions to fragment was also found to be an important factor in ESI. When probing peptides and related systems, increasing the sample cone potential typically leads to in-source fragmentation (sometimes referred to as nozzle skimmer dissociation), whereas MOSs tend to remain

intact under the same conditions in the positive mode. This behavior is illustrated in the uppermost plot of Fig. 2. At cone potentials below 75 V, significant losses of carbohydrate signal were experienced in the positive mode, whereas higher cone potentials produced signals approximately 10 times more intense. Interestingly, high cone potentials in the negative mode also produced an abundance of signal. However, the primary carbohydrate series did not correspond to an intact molecular ion. Rather, this series was the result of in-source fragmentation corresponding to the loss of 120.0423 Da ( $C_4H_8O_4$ ) from the deprotonated species to yield  $[M-C_4H_8O_4-H]^-$  as reported by Yamagaki and Nakanishi [31]. These ions correspond to deprotonated  $^{0,2}X$  or  $^{2,4}A$  fragments of the MOS ions. Lowering the cone potential to 60 V virtually eliminated the

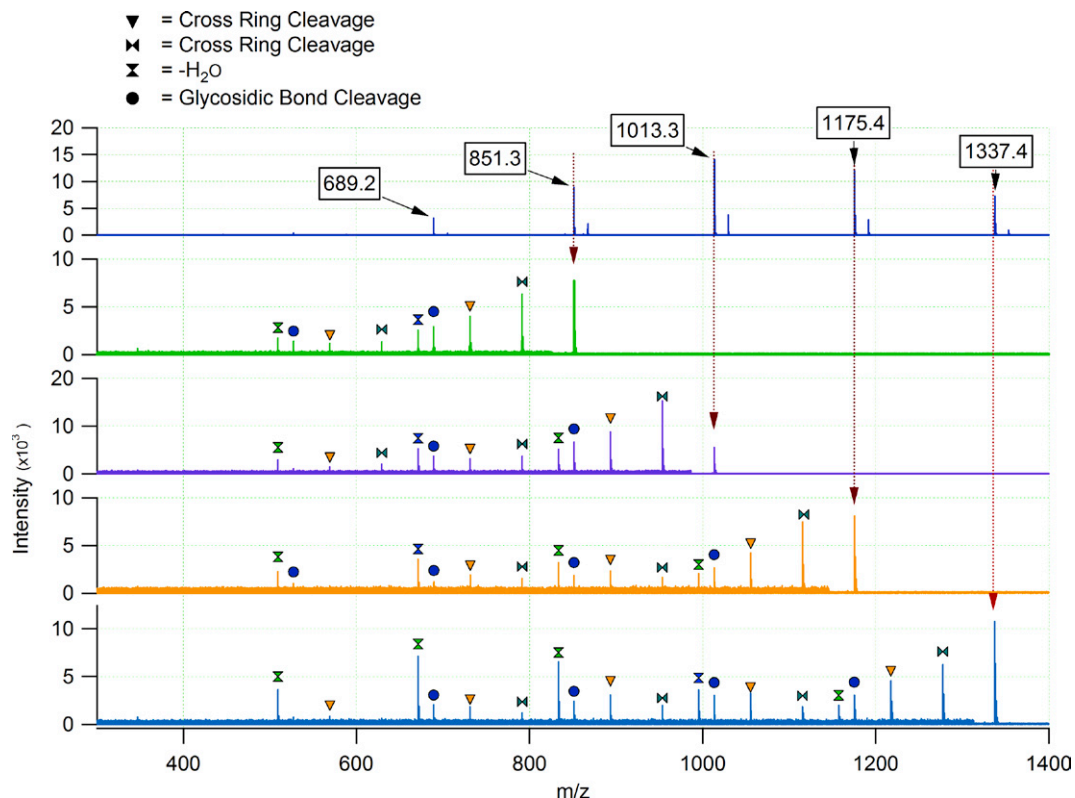


**Fig. 3.** ESI-FT-ICR tandem MS with IRMPD of selected beer MOSs. The vertical dotted lines provide a visual guide to the parent ion masses. The remaining peaks resulted from the IRMPD of the precursor ions and represented either the loss of water or cross-ring cleavage (see legend on figure). The  $m/z$  region of each spectrum below the parent ion has been magnified for clarity.

in-source fragmentation and allowed the deprotonated  $[M-H]^-$  ions of the MOSs to dominate (Fig. 2, lower trace). Overall, the

signal for beer MOSs was maximized using a high cone potential ( $\sim 95V$ ) in the positive mode and a lower cone potential ( $\sim 60V$ ) in

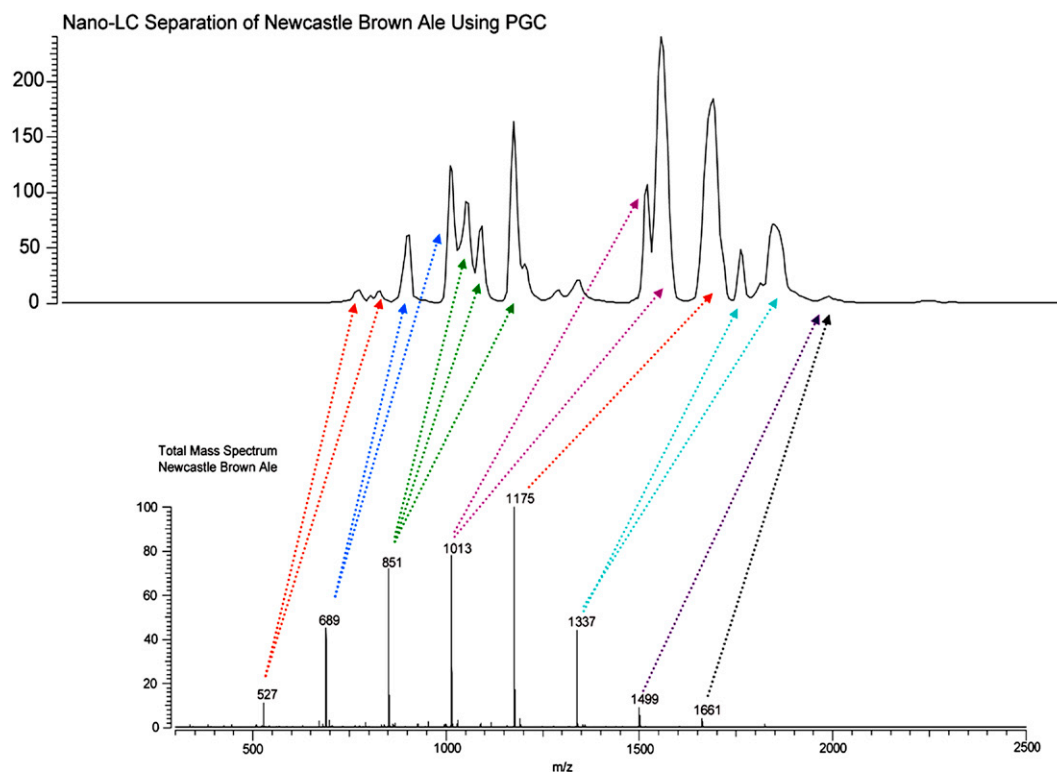


**Fig. 4.** Annotated nano-LC/FT-ICR-MS separation of MOSs derived from beer. Using PGC as the stationary phase, singular  $m/z$  values within multiple nano-LC elution peaks were often observed, indicating the presence of isomeric carbohydrates.

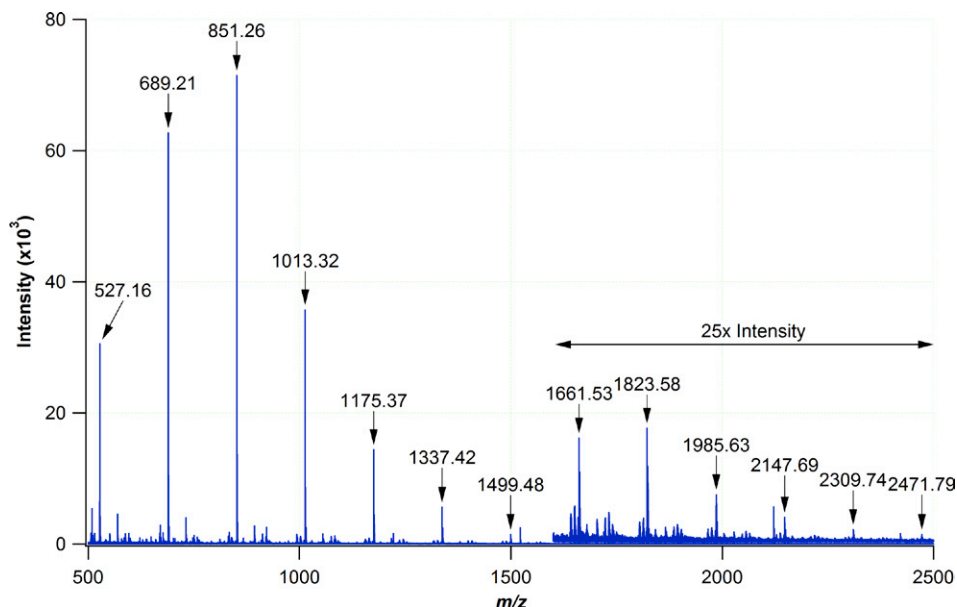


**Fig. 5.** Positive ion mode ESI-TOF-MS analysis of PGC-purified beer MOSs with an effective dilution factor of 100. Above  $m/z$  1600, the intensity scale has been expanded by a factor of 25 for clarity. The major MOS series corresponds to  $[M+Na]^+$  ions.

the negative mode. Although the possibility of in-source fragmentation at higher cone potentials cannot be eliminated entirely, this occurrence seems less likely when considering all data obtained for each MOS sample in both the positive and negative modes. As Fig. 2 illustrates, softening the environment of the atmospheric pressure interface in the negative mode allowed intact molecular ions to be observed. Using these same source parameters in the positive mode failed to produce the protonated species or appreciable amounts of metal adducted carbohydrate ions. Because it was unlikely that higher cone potentials induced the formation of alkali earth adducts, cone potentials above approximately 75 V were evidently necessary to adequately desolvate the sodium and potassium adducts of MOSs prior to mass analysis. Previous work examining the conformation of metal-coordinated carbohydrates

has demonstrated the ability of the metal ions to coordinate with multiple oxygen atoms simultaneously [26,32]. This serves to provide an explanation for the absence of in-source fragmentation in positive mode ESI of MOS alkali metal adducts.

Although in-source fragmentation was not observed for the metal-coordinated MOSs produced in positive mode ESI, detailed tandem MS experiments were possible using IRMPD. As shown in Fig. 3, the fragments observed for MOSs corresponded to loss of water, glycosidic bond cleavage, and two subsequent cross-ring cleavages. For carbohydrates in particular, IRMPD typically provides a wealth of information that may be used to confirm oligosaccharide composition. However, these compositional assignments do not preclude the possibility of isomerism. It is believed that MOSs derived from beer are composed primarily of linear carbo-

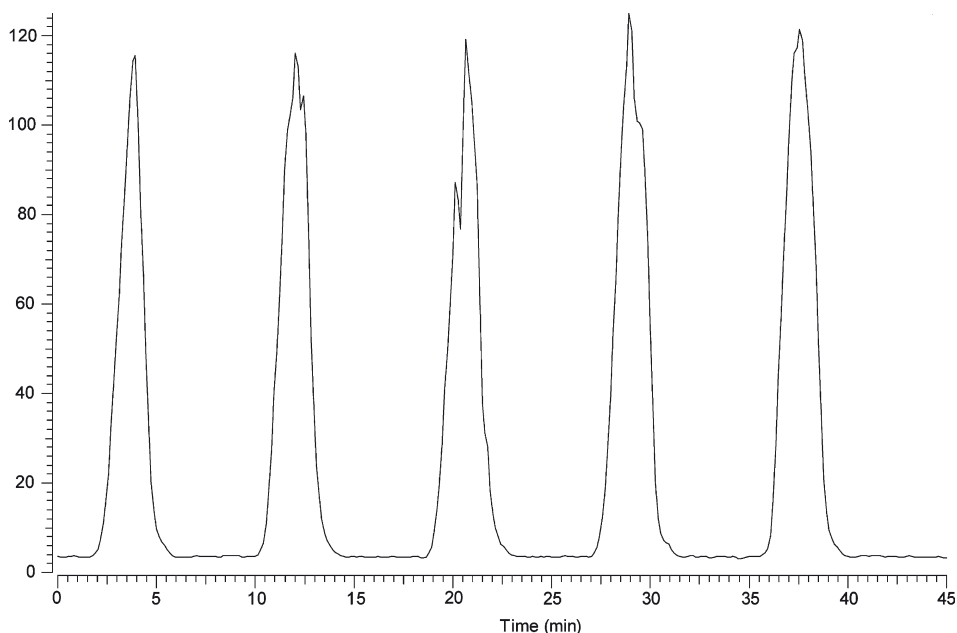


**Fig. 6.** Infusion of beer MOSs using ESI-FT-ICR-MS. The plot of total ion intensity observed over time illustrates the reproducible nature of five 1- $\mu$ l beer MOS injections and the lack of carryover between samples.

hydrates, although nano-LC separation using PGC as the stationary phase illustrates the possibility of isomers.

Fig. 4 shows the annotated nano-LC chromatogram of beer-derived MOS and the corresponding mass spectrum summed across the entire chromatographic run. Interestingly, the chromatogram contains many more peaks than the eight primary  $m/z$  ratios found in the summed mass spectrum for the nano-LC experiment. The multiplicity of chromatographic peaks in comparison with the mass spectral signals suggests the presence of isobaric but structurally distinct carbohydrate species in beer. Despite the presence of MOS isomers, the utility of these compounds as mass calibrants remains intact due to the inability of MS to resolve truly isobaric ions.

Although the MOSs found in samples of dilute beer are readily detected by FT-ICR-MS, the ability to produce and detect these ions is not unique to that particular mass analyzer. As demonstrated in Fig. 5, the MOSs are readily observed as sodium adducts in positive ion mode ESI-TOF-MS. Thus, MOS series not only are useful due to dual polarity accessibility in both ESI and MALDI, but also provide calibration and tuning standards well suited to the optimization of various types of mass spectrometers for carbohydrate analysis. It should be noted that to increase the detection of these ions with a good signal-to-noise ratio, the source conditions (voltages) were altered from those typically used for proteomics.

In addition to their ease of use, compatibility with ESI and MALDI, and fairly comprehensive mass range in either polarity, perhaps the most attractive feature of beer MOSs is their lack of memory effects. Fig. 6 highlights the lack of carryover associated with the use of beer MOSs as tuning standards for MS. Five 1- $\mu$ l injections were performed at 8-min intervals with a flow rate of 500 nl/min. Under these conditions and with the flow rate held constant, the total ion signal returned to baseline shortly after injection. No special effort was made to flush the MOSs from the system. At no time during the course of this study were the electrospray emitters replaced due to contamination with MOSs. It should also be noted that through refrigeration, the integrity of the stock solution was maintained for periods lasting many months.

## Conclusions

Using nano-ESI and MALDI as ionization sources with FT-ICR-MS and TOF-MS as mass analyzers, beer MOSs have been successfully used as mass calibrants and tuning standards in both the positive and negative ion modes. Because the MOSs are derived from beer, the mass calibration and tuning range are not limited by the commercial unavailability of pure MOSs with sufficiently high DPs. Relatively high cone voltages in positive mode nano-ESI favored the production of sodium and potassium adducts, whereas the same settings in the negative mode induced cross-ring cleavage. This in-source fragmentation was alleviated by lowering the cone potential to produce the deprotonated molecular ions of beer MOSs. These source conditions are typical for oligosaccharide analysis using nano-ESI in our research group. With ionization by MALDI and using DHB as the matrix, sample spots doped with NaCl almost exclusively produced MOS ions as sodium adducts in the positive ion mode. When operating in negative mode MALDI and using harmine/NH<sub>4</sub>Cl as the matrix, the MOSs were observed primarily as internal fragments resulting from sequential cross-ring cleavages at both termini, but they remained useful as mass and tuning standards because the elemental composition of the fragments could be deduced.

Although MOS content varied slightly with the selected beer, the overall composition and, more important, the  $m/z$  ratios observed remained constant. The stringent level of quality control for these products results in highly reproducible MOS distributions for any given brand. In addition to being amenable to dual polarity

ionization using both ESI and MALDI, beer MOSs are easily enriched, cost-effective, readily available, amenable for carbohydrate analysis, and relatively comprehensive calibrants ( $m/z \geq 500$ –2500) that do not suffer from memory effects that hinder many traditional mass and tuning standards.

## Acknowledgments

The authors thank Agilent Technologies for use of the 6200 series HPLC chip/TOF-MS. The following funding sources are also acknowledged: Dairy Management Incorporated California Dairy Research Foundation (06 LEC-01-NH), University of California Discovery Grant (05GEB01NHB), and National Institutes of Health (GM 49077).

## References

- [1] D.L. Lawrence, Accurate mass measurement of positive ions produced by ammonia chemical ionization, *Rapid Commun. Mass Spectrom.* 4 (1990) 546–549.
- [2] K.R. Jonscher, J.R. Yates III, Mixture analysis using a quadrupole mass filter/quadrupole ion trap mass spectrometer, *Anal. Chem.* 68 (1996) 659–667.
- [3] L. Jiang, M. Moini, Ultramark 1621 as a reference compound for positive and negative ion fast-atom bombardment high-resolution mass spectrometry, *J. Am. Soc. Mass Spectrom.* 3 (1992) (1621) 842–846.
- [4] R.P. Lattimer, Fast atom bombardment mass spectrometry of polyglycols, *Int. J. Mass Spectrom. Ion Proc.* 55 (1984) 221–232.
- [5] L.J. Goad, M.C. Prescott, M.E. Rose, Poly(ethyleneglycol) as a calibrant and solvent for fast atom bombardment mass spectrometry: application to carbohydrates, *Org. Mass Spectrom.* 19 (1984) 101–104.
- [6] R.P. Lattimer, Tandem mass spectrometry of lithium-attachment ions from polyglycols, *J. Am. Soc. Mass Spectrom.* 3 (1992) 225–234.
- [7] K. Vekey, Calibration in positive and negative ion fast atom bombardment using salt mixtures, *Org. Mass Spectrom.* 24 (1989) 183–185.
- [8] S. Konig, H.M. Fales, Calibration of mass ranges up to  $m/z$  10,000 in electrospray mass spectrometers, *J. Am. Soc. Mass Spectrom.* 10 (1999) 273–276.
- [9] J.B. Fenn, M. Mann, C.K. Meng, S.F. Wong, C.M. Whitehouse, Electrospray ionization for mass spectrometry of large biomolecules, *Science* 246 (1989) 64–71.
- [10] K. Tanaka, H. Waki, Y. Ido, S. Akita, Y. Yoshida, T. Yohida, Protein and polymer analyses up to  $m/z$  100,000 by laser ionization time-of-flight mass spectrometry, *Rapid Commun. Mass Spectrom.* 2 (1988) 151–153.
- [11] M. Moini, Ultramark 1621 as a calibration/reference compound for mass spectrometry: II. Positive- and negative-ion electrospray ionization, *Rapid Commun. Mass Spectrom.* 8 (1994) (1621) 711–714.
- [12] R.B. Cody, J. Tamura, B.D. Musselman, Electrospray ionization magnetic sector mass spectrometry: calibration, resolution, and accurate mass measurements, *Anal. Chem.* 64 (1992) 1561–1570.
- [13] C.N. McEwen, B.S. Larsen, Accurate mass measurement of proteins using electrospray ionization on a magnetic sector instrument, *Rapid Commun. Mass Spectrom.* 6 (1992) 173–178.
- [14] W.A. Harris, D.J. Jannecki, J.P. Reilly, Use of matrix clusters and trypsin autolysis fragments as mass calibrants in matrix-assisted laser desorption/ionization time-of-flight mass spectrometry, *Rapid Commun. Mass Spectrom.* 16 (2002) 1714–1722.
- [15] S. Konig, H.M. Fales, Formation and decomposition of water clusters as observed in a triple quadrupole mass spectrometer, *J. Am. Soc. Mass Spectrom.* 9 (1998) 814–822.
- [16] E. Vinogradov, K. Bock, Structural determination of some new oligosaccharides and analysis of the branching pattern of isomaltooligosaccharides from beer, *Carbohydr. Res.* 309 (1998) 57–64.
- [17] P. Mauri, M. Minoggio, P. Simonetti, C. Gardana, P. Pietta, Analysis of saccharides in beer samples by flow injection with electrospray mass spectrometry, *Rapid Commun. Mass Spectrom.* 16 (2002) 743–748.
- [18] A.S. Araujo, L.L. da Rocha, D.M. Tomazela, A.C.H.F. Sawaya, R.R. Almeida, R.R. Catharino, M.N. Eberlin, Electrospray ionization mass spectrometry fingerprinting of beer, *Analyst* 130 (2005) 884–889.
- [19] S. Cortacero-Ramirez, A. Segura-Carretero, C. Cruces-Blanco, M. Hernainz-Bermudez de Castro, A. Fernandez-Gutierrez, Analysis of carbohydrates in beverages by capillary electrophoresis with precolumn derivatization and UV detection, *Food Chem.* 87 (2004) 471–476.
- [20] L.C. Nogueira, F. Silva, I.M.P.L.V.O. Ferreira, L.C. Trugo, Separation and quantification of beer carbohydrates by high-performance liquid chromatography with evaporative light scattering detection, *J. Chromatogr. A* 1065 (2005) 207–210.
- [21] K. Bock, T. Dreyer, S. Mueller-Loennies, L. Molskov-Bech, Evaluation of new analytical techniques for the optimization of brewing processes, *Proc. Inst. Brew.* 24 (1996) 234–238.
- [22] I.F. Duarte, M. Spraul, M. Godejohann, U. Braumann, M. Spraul, A.M. Gil, Application of NMR spectroscopy and LC-NMR/MS to the identification of carbohydrates in beer, *J. Agric. Food Chem.* 51 (2003) 4847–4852.
- [23] N.H. Packer, M.A. Lawson, D.R. Jardine, J.W. Redmond, A general approach to desalting oligosaccharides released from glycoproteins, *Glycoconj. J.* 15 (1998) 737–747.



- [24] M.J. Davies, K.D. Smith, R.A. Carruthers, W. Chai, A.M. Lawson, E.F. Hounsell, Use of a porous graphitized carbon column for the high-performance liquid chromatography of oligosaccharides, alditols, and glycopeptides with subsequent mass spectrometry analysis, *J. Chromatogr.* 646 (1993) 317–326.
- [25] H. Suzuki, T. Yamagaki, K. Tachibana, Optimization of matrix and amount of ammonium chloride additive for effective ionization of neutral oligosaccharides as chloride ion adducts in negative-mode MALDI–TOF mass spectrometry, *J. Mass Spectrom. Soc. Jpn.* 53 (2005) 227–229.
- [26] M.T. Cancilla, S.G. Penn, J.A. Carroll, C.B. Lebrilla, Coordination of alkali metals to oligosaccharides dictates fragmentation behavior in matrix assisted laser desorption/ionization/Fourier transform mass spectrometry, *J. Am. Chem. Soc.* 118 (1996) 6736–6745.
- [27] T.R.I. Cataldi, C. Campa, G.E. de Benedetto, Carbohydrate analysis by high-performance anion-exchange chromatography with pulsed amperometric detection: the potential is still growing, *Fresenius J. Anal. Chem.* 368 (2000) 739–758.
- [28] R.B. Cole, J. Zhu, Chloride anion attachment in negative ion electrospray ionization mass spectrometry, *Rapid Commun. Mass Spectrom.* 13 (1999) 607–611.
- [29] T. Yamagaki, H. Suzuki, K. Tachibana, In-source and postsource decay in negative-ion matrix-assisted laser desorption/ionization time-of-flight mass spectrometry of neutral oligosaccharides, *Anal. Chem.* 77 (2005) 1701–1707.
- [30] B. Domon, C.E. Costello, A systematic nomenclature for carbohydrate fragmentations in FAB–MS/MS spectra of glycoconjugates, *Glycoconj. J.* 5 (1988) 397–409.
- [31] T. Yamagaki, H. Nakanishi, Negative-mode matrix-assisted laser desorption/ionization mass spectrometry of maltoheptaose and cyclomaltooligosaccharides, *J. Mass Spectrom. Soc. Jpn.* 50 (2002) 204–207.
- [32] G.E. Hofmeister, Z. Zhou, J.A. Leary, Linkage position determination in lithium-cationized disaccharides: tandem mass spectrometry and semiempirical calculations, *J. Am. Chem. Soc.* 113 (1991) 5964–5970.